APPLIED PHYSICS LETTERS **86**, 082110 (2005)

Enhancement of *p*-type conductivity in nanocrystalline $BaTiO_3$ ceramics

Xin Guo,[a] Christian Pithan, Christian Ohly, and Chun-Lin Jia
Institut für Festkörperforschung, Forschungszentrum Jülich, 52425 Jülich, Germany

Jügen Dornseiffer and Franz-Hubert Haegel
Institut für Chemie und Dynamik der Geosphäre, Forschungszentrum Jülich, 52425 Jülich, Germany

Rainer Waser
Institut für Festkörperforschung, Forschungszentrum Jülich, 52425 Jülich, Germany

(Received 10 August 2004; accepted 16 December 2004; published online 18 February 2005)

Undoped $BaTiO_3$ ceramic samples with an average grain size of ~35 nm were prepared and the electrical properties investigated. The defect structure is dominated by acceptor impurities; therefore, the conductivity of nanocrystalline $BaTiO_3$ is of *p*-type. Comparing with microcrystalline $BaTiO_3$, the conductivity of nanocrystalline $BaTiO_3$ is about 1 to 2 orders of magnitude higher and the activation energy remarkably lower, which is ascribed to a greatly reduced oxidation enthalpy in nanocrystalline $BaTiO_3$ (~0.3 versus ~0.92 eV for microcrystalline $BaTiO_3$). © *2005 American Institute of Physics*. [DOI: 10.1063/1.1864232]

In the last few years, a number of dense nanocrystalline oxides, for example, undoped and Gd_2O_3-doped CeO_2 with an average grain size of ~10 nm,[1,2] ~11–36 nm,[3] ~26 (Ref. 4) and ~30 nm,[5] respectively, undoped TiO_2 with an average grain size of ~35 nm,[6] and Y_2O_3-doped ZrO_2 with an average grain size of ~20,[7] ~41,[8] and ~50 nm,[9] respectively, either in bulk form or thin-film form, have been prepared and the electrical properties investigated. Among these nanocrystalline oxides, the most dramatic property changes were observed for nanocrystalline CeO_2. Comparing with microcrystalline counterparts, nanocrystalline CeO_2 is characterized by an orders-of-magnitude enhanced *n*-type conductivity and a significantly reduced activation energy. This phenomenon was explained by a greatly reduced reduction enthalpy of nanocrystalline CeO_2, and the grain-boundary sites of lower vacancy formation enthalpy were proposed to be the atomic-level origin of this behavior.[1,2] However, Kim and Maier[5] proposed that the higher conductivity of nanocrystalline CeO_2 is due to the electron accumulation at the grain boundaries. With its comparatively high electronic bulk contribution and high density of grain boundaries, the grain boundaries in nanocrystalline CeO_2 can become electronically conducting and dominate the overall behavior.

Nanocrystalline $BaTiO_3$ materials of high density have also been prepared in thin-film form with an average grain size of ~25 nm,[10] and in bulk form with an average grain size of ~70 nm,[11] respectively, and the ferroelectric properties characterized. It is found that the ferroelectricity is weakened and the dielectric constant is remarkably lower for nanocrystalline $BaTiO_3$ ceramics.[11] The ferroelectric response is even absent when the grain size is 25 nm.[10] In neutral to oxidizing atmospheres, acceptor-doped $BaTiO_3$ shows a *p*-type conductivity.[12,13] In this letter, the defect and transport properties of nanocrystalline $BaTiO_3$ ceramics, nominally undoped but actually doped with acceptor impurities, are characterized, featuring an enhanced *p*-type conductivity.

$BaTiO_3$ powder with an average particle diameter of ~10 nm was synthesized through the hydrolytic decomposition of a barium-titanium-isopropoxide solution in a water-in-oil microemulsion, consisting of 10.47 wt. % of Tergitol NP35, 80.70 wt. % of cyclohexane, 6.04 wt. % of 1-octanol and 2.79 wt. % of ultrapure and degassed water. Since the reaction is confined to the ultrasmall space of individual aqueous micelles, this approach allows the formation of nanopowders.[14] The Ti/Ba ratio of the powder was determined to be 1.0035 ± 0.0004 by x-ray fluorescence spectroscopy. According to inductively coupled plasma mass spectroscopy analyses, the nominally undoped $BaTiO_3$ powder was actually doped with acceptor impurities (mainly 82 ppm Mn, the others, e.g., Al, Sc, Fe, etc., are below the detection limit). The powder was densified by hot isostatic pressing at 860 °C under 200 MPa in nitrogen. The density of the ceramic pellets thus obtain was about 93% of the theoretical density. Figure 1 shows the transmission electron micrograph (Model JEOL 4000EX, operating at 400 kV) of the nanocrystalline $BaTiO_3$ ceramic, indicating an average grain size of ~35 nm. The high-resolution transmission electron micrograph shown in the inset demonstrates that the grain boundaries were free of impurity phases. For comparison, microcrystalline samples with an average grain size of ~5.6 μm were prepared by firing the nanocrystalline samples at 1100 °C for 2 h.

The electrical properties were investigated by impedance spectroscopy performed at an amplitude of 100 mV (model 1260 frequency response analyzer, Solartron Instruments). Within the frequency range of 0.1 to 10^7 Hz, normally two relaxation processes (semicircles) were recorded in the impedance spectra of the microcrystalline sample (Fig. 2). In the order of decreasing frequency, the two semicircles correspond to the impedance responses of the bulk and the grain boundaries,[15] respectively. The impedance spectra were fitted according to an equivalent circuit consisting of two *RQ* (*R*: resistance, *Q*: constant phase element) circuits in series. In contrast, within the same frequency range only one distorted arc was recorded in the impedance spectra of the nanocrys-

[a]Author to whom correspondence should be addressed; present address: Department of Materials Science and Engineering, University of Florida, P.O. Box 116400, Gainesville, Florida 32611-6400; electronic mail: xinguo@ufl.edu

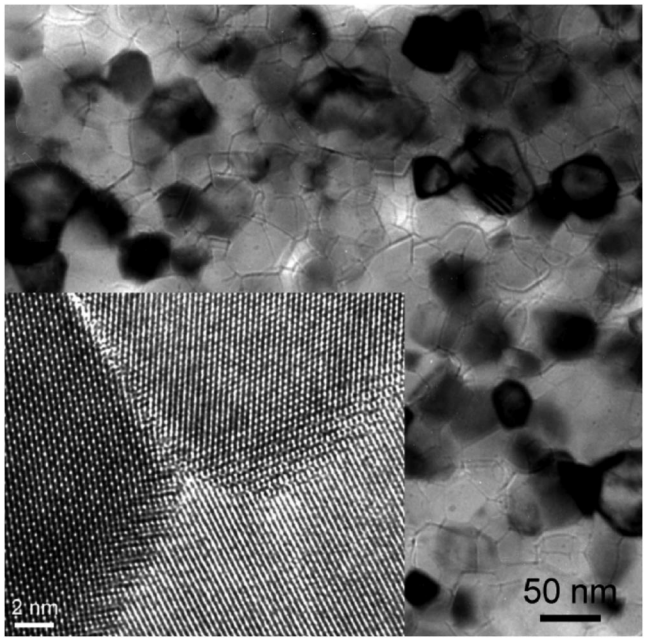

FIG. 1. Transmission electron micrograph of $BaTiO_3$ ceramic with an average grain size of ~35 nm. The high-resolution transmission electron micrograph shown in the inset demonstrates atomically abrupt grain boundaries with no intergranular impurity phase.

talline sample. The arc was fitted by a large high-frequency semicircle and a small low-frequency semicircle (Fig. 2). In nanocrystalline materials, the grain boundaries parallel to the current direction, the contribution of which is negligible in microcrystalline materials, make considerable contribution to the impedance.[16] The high-frequency semicircle in the impedance spectrum of the nanocrystalline $BaTiO_3$ sample most probably results from the superposition of the bulk and the parallel grain boundaries, whereas, the low-frequency semicircle may come from the perpendicular grain boundaries that are still blocking the charge carrier transport across the grain boundaries. From the intersections of the fitted semicircles on the real axis, the bulk resistance and the total (bulk plus grain boundary) resistance can be obtained, and then the electrical conductivity is simply $L/(RA)$. Here L is the sample thickness, and A the cross-section area. The electrical conductivities of the nano- and microcrystalline $BaTiO_3$ ceramics measured in pure oxygen ($P_{O_2}=10^5$ Pa) are plotted in Fig. 3 as a function of temperature. Within the

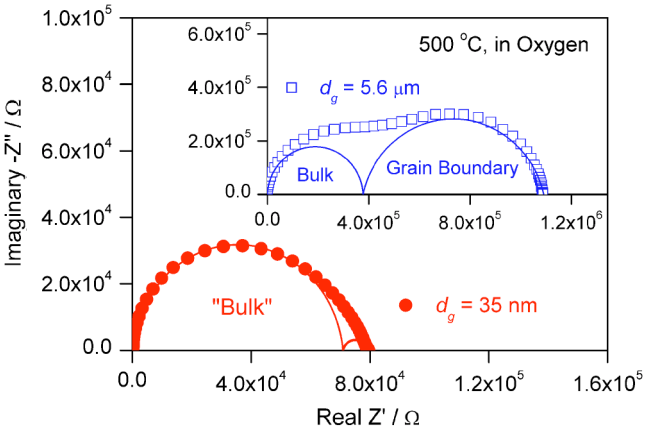

FIG. 2. Typical impedance spectra for nano- and microcrystalline $BaTiO_3$ samples measured at 500 °C in pure oxygen.

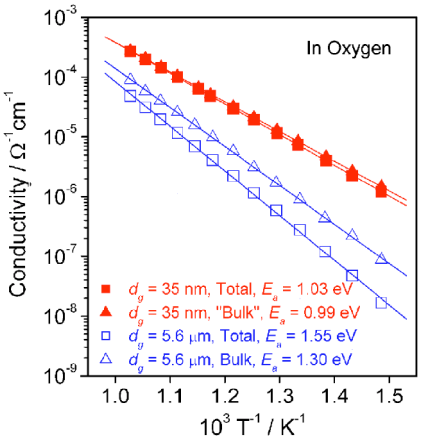

FIG. 3. Temperature dependence of the conductivities of nano- and microcrystalline $BaTiO_3$ samples measured in pure oxygen.

temperature range of 400 to 700 °C, the conductivity of the nanocrystalline sample is about one to two orders of magnitude higher than that of the microcrystalline sample, and the activation energy is remarkably lower for the nanocrystalline sample. After the impedance measurements, the average grain size of the nanocrystalline sample was checked again, and it was determined to be ~39.5 nm from the full width at half-maximum of the (200) peak using the Scherrer formula, demonstrating no grain growth during the electrical measurements.

As the samples are doped with acceptor impurities, the principal defect reaction in an oxidizing atmosphere is[12,13]

$$V_O^{\cdot\cdot} + 1/2O_2 \leftrightarrow O_O^x + 2h^{\cdot}, \tag{1a}$$

$$K_{Ox}(T) = \frac{p^2}{[V_O^{\cdot\cdot}]P_{O_2}^{1/2}} = K_{Ox}^0 \exp\left(-\frac{\Delta H_{Ox}}{k_B T}\right). \tag{1b}$$

In Eq. (1b), ΔH_{Ox} is the oxidation enthalpy, k_{Ox}^0 the preexponential constant, k_B the Boltzmann constant, T the absolute temperature, P_{O_2} the oxygen partial pressure, p and $[V_O^{\cdot\cdot}]$ are the concentrations of holes ($h^{\cdot}$) and oxygen vacancies ($V_O^{\cdot\cdot}$), respectively. Owing to the higher mobility of holes, the conductivity of the nanocrystalline sample is of p-type, as demonstrated by the oxygen partial pressure dependence (Fig. 4). Although a similar electron accumulation at the grain boundaries is expected for acceptor-doped $BaTiO_3$ [as proved for acceptor-doped $SrTiO_3$ (Ref. 17)], the higher con-

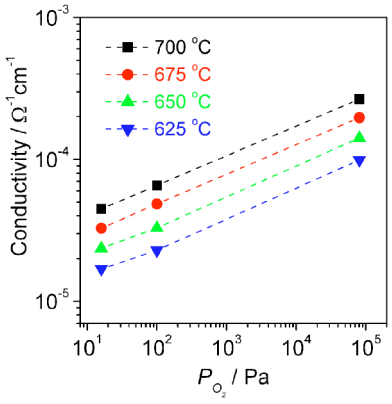

FIG. 4. Oxygen partial pressure dependence of the bulk conductivity of nanocrystalline $BaTiO_3$.

ductivity of nanocrystalline $BaTiO_3$ shown in Fig. 3 cannot be due to the electron accumulation at the grain boundaries; this is because of the *p*-type conductivity of nanocrystalline $BaTiO_3$.

At 700 °C, both the nano- and microcrystalline samples were annealed under $P_{O_2}=2$ Pa for 30 h, afterwards, pure oxygen was introduced and both samples were annealed in oxygen for another 30 h. This treatment caused a weight gain of ~0.023 wt. % in the microcrystalline sample, whereas ~0.098 wt. % in the nanocrystalline sample. This phenomenon suggests that the $K_{Ox}(T)$ value of Eq. (1b) is higher for nanocrystalline $BaTiO_3$, which may be due to a smaller oxidation enthalpy for nanocrystalline $BaTiO_3$. From Eq. (1b), one readily gets $p \sim \exp(-\Delta H_{Ox}/2k_BT)$. In addition, the mobility $\mu \sim \exp(-\Delta H_m/k_BT)$, so that the conductivity $\sigma \sim \exp[-(\Delta H_{Ox}/2+\Delta H_m)/k_BT]$ as $\sigma=ep\mu$; therefore, the activation energy for the *p*-type conductivity $E_a=\Delta H_{Ox}/2+\Delta H_m$. In these equations, ΔH_m is the migration enthalpy of holes, and *e* the elementary charge. For microcrystalline $BaTiO_3$, ΔH_{Ox} was determined to be ~0.92 eV.[12] Assuming that ΔH_m is similar for micro- and nanocrystalline $BaTiO_3$, one estimates ΔH_{Ox} to be ~0.3 eV for nanocrystalline $BaTiO_3$ from the activation energies for the bulk conductivities given in Fig. 3. This indicates an amazing reduction of the oxidation enthalpy. A smaller ΔH_{Ox} for nanocrystalline $BaTiO_3$ naturally results in a higher hole concentration and higher *p*-type conductivity.

Nanocrystalline $BaTiO_3$ is supposed to consist of ferroelectric grains and nonferroelectric grain boundaries.[11] Usually the grain boundaries are suggested to be cubic or pseudocubic.[18,19] Owing to the very high volume fraction of the grain boundaries in nanocrystalline materials, nanocrystalline $BaTiO_3$ presumes a pseudocubic structure even at room temperature, according to x-ray diffraction analyses. The grain-boundary region is expected to be distorted, which may facilitate the defect reaction given in Eq. (1) (i.e., smaller ΔH_{Ox}). At nanometer scale, the defect thermodynamics of $BaTiO_3$ is most probably dominated by the grain boundaries.

In conclusion, the *p*-type conductivity of nanocrystalline $BaTiO_3$ is about 1 to 2 orders of magnitude higher than that of microcrystalline counterparts, and the activation energy is lower. This phenomenon can be explained by a significantly reduced oxidation enthalpy of nanocrystalline $BaTiO_3$.

[1] Y.-M. Chiang, E. B. Lavik, I. Kosacki, H. L. Tuller, and J. Y. Ying, Appl. Phys. Lett. **69**, 185 (1996).
[2] Y.-M. Chiang, E. B. Lavik, I. Kosacki, H. L. Tuller, and J. Y. Ying, J. Electroceram. **1**, 7 (1997).
[3] T. Suzuki, I. Kosacki, and H. U. Anderson, J. Am. Ceram. Soc. **85**, 1492 (2002).
[4] A. Tschöpe, E. Sommer, and R. Birringer, Solid State Ionics **139**, 255 (2001).
[5] S. Kim and J. Maier, J. Electrochem. Soc. **149**, J73 (2002).
[6] P. Knauth and H. L. Tuller, J. Appl. Phys. **85**, 897 (1999).
[7] I. Kosacki, T. Suzuki, V. Petrovsky, and H. U. Anderson, Solid State Ionics **136–137**, 1225 (2000).
[8] P. Mondal, A. Klein, W. Jaegermann, and H. Hahn, Solid State Ionics **118**, 331 (1999).
[9] Y. W. Zhang, S. Jin, Y. Yang, G. B. Li, S. J. Tian, J. T. Jia, C. S. Liao, and C. H. Yan, Appl. Phys. Lett. **77**, 3409 (2000).
[10] M. H. Frey and D. A. Payne, Appl. Phys. Lett. **63**, 2753 (1993).
[11] M. H. Frey, Z. Xu, P. Han, and D. A. Payne, Ferroelectrics **206–207**, 337 (1998).
[12] N.-H. Chan, R. K. Sharma, and D. M. Smyth, J. Am. Ceram. Soc. **64**, 556 (1981).
[13] N.-H. Chan, R. K. Sharma, and D. M. Smyth, J. Am. Ceram. Soc. **65**, 167 (1982).
[14] H. Herrig and R. Hempelmann, Nanostruct. Mater. **9**, 241 (1997).
[15] N. Hirose and A. R. West, J. Am. Ceram. Soc. **79**, 1633 (1996).
[16] J.-H. Hwang, D. S. Mclachlan, and T. O. Mason, J. Electroceram. **3**, 7 (1999).
[17] R. Hagenbeck and R. Waser, J. Appl. Phys. **83**, 2083 (1998).
[18] G. Arlt, D. Hennings, and G. de With, J. Appl. Phys. **58**, 1619 (1985).
[19] T. Takeuchi, K. Ado, T. Asai, H. Kageyama, Y. Saito, C. Masquelier, and O. Nakamura, J. Am. Ceram. Soc. **77**, 1665 (1994).